# Supporting information

## Novel Synthesis Approach of Metal-Biomolecule-Hexacyanoferrate Composite Nanofibers besides Developing a Chiral Sensing Probe

*Seyedeh Fatemeh Nami-Ana[A], Javad Tashkhourian[A]*, Mojtaba Shamsipur[B]*

*[A] Department of Chemistry, College of Sciences, Shiraz University, Shiraz 71456, Iran*

*[B] Department of Chemistry, Razi University, Kermanshah, Iran*

**Experimental:**

**S1. Preparation of CuO nanoparticles**

Copper oxide (CuO) nanoparticles prepared according to the method reported in literature using an alcothermal process. A precipitation reaction between copper actate( $Cu(CH_3COO)_2$)with the concentration of 25 mM and NaOH concentration of 100 mM in ethanol at 78 ◦C for 1 h the orange-brown color of nanoparticles formed. It is on the basis of the following reaction: Cu $(CH_3COO)_2$ + 2NaOH → CuO + 2Na$(CH_3COO)_2$ + $H_2O$ The prepared particles washed with ethanol and centrifuged to remove the by-products**.**

**S2. Preparation of Copper Nanoclusters**

The glutathione (GSH) protected sub nanometer zized CuNCs prepared by a one-pot method.[1] Briefly, 21.5 mg of $CuCl_2$. $2H_2O$ (Merck) dissolved in 2.5 ml of aqueous solution and added to the 2.5 ml solution containing 76.5 mg GSH(Merck) under vigorous stirring. The pH value dropped to 2–3,then, 250.0 µl of 5.0 mM sodium hydroxide solution (Merck) introduced into the reaction mixture with a slow stirring speed. After 10 min, 0.5 ml of hydrazine hydrate (Merck) added drop wise to the mixture. The color of the solution is changed in half an hour from colorless to yellow-green, and then to gold yellow. After three hours of stirring, the reaction flask moved to the fridge and aged 12 h to obtain stable CuNCs. The finally obtained nanoclusters purified by adding ethanol in the cyclic method of precipitation and centrifugation and dissolved in 2.0 ml water and stored [1]. 10.0, 20.0 and 30. 0 mg of the suspensions are mixed with the graphite powder and dried in 40°C, then are used to prepare carbon paste electrodes.

**S3. Preparation of $Cu_2O$ nanocube**

In a typical synthesis reported by S. Badhulika et al.[2], 0.169 g of $CuCl_2.{}_2H_2O$ (0.012 M) was dissolved into 50 mL water and the solution put under vigorous stirring at 60 °C which gives a blue color solution. When the $CuCl_2.2H_2O$ gets dissolved completely as a homogenous solution, 10 mL of 2 M sodium hydroxide (NaOH) was added slowly to the solution for precipitation giving rise to intense blue color. After 30 min of stirring under 60 °C, 10 mL of 0.6 M L-Ascorbic acid (AA) was added dropwise into the solution and kept under vigorous stirring for 3 h for reduction. The solution immediately turns into yellow color and then to brick-red indicating the formation of $Cu_2O$ nanocubes.

**S4. Chemical synthesis of CuHCF**

CuHCF was prepared as follow: 200mg of Cu-L-As nanofibers was dispersed in a 50 mL aqueous solution and then, 100 mL aqueous solution of $K_3[Fe(CN)_6]$ (0.005 M) was added dropwise into Cu-L-As nanofibers suspension. The mixture was stirred for 6 h and then the resulting precipitate was filtered. The dark brown solid precipitate was then dried in an oven at 85C for 12 h. The obtained CuHCFe, was collected for further uses and named as chemically synthesized-CuHCF.

**S5. Raman Spectral Analysis**

The Raman spectrum of L-aspartic acid nanofiber displayed in Figure S7 B. It is dominated by internal vibrational modes of the carboxylate and amino groups in the fingerprint region (300–1600 $cm^{-1}$), while low-frequency bands observed at approximately 139 and 190 $cm^{-1}$ are assigned to lattice modes. These low-wavenumber features originate from collective intermolecular vibrations, including translational and rotational motions of zwitterionic aspartic acid units stabilized by hydrogen bonding within the crystal lattice, rather than from specific intramolecular functional group vibrations. Such low-frequency Raman modes are well documented for amino acid crystals and are highly sensitive to crystal packing and long-range order. Upon coordination of aspartate ligands to $Cu^{2+}$ ions, the carboxylate stretching bands shift and split, consistent with metal–carboxylate coordination, a sharp peak appears at 485 $cm^{-1}$ while additional weak features appear in the 400–600 $cm^{-1}$ region corresponding to Cu–O/Cu–N vibrations. In the ternary Cu–hexacyanoferrate system, new intense Raman bands emerge in the 2000–2200 $cm^{-1}$ region, which are unambiguously assigned to the $\nu(C\equiv N)$

stretching modes of hexacyanoferrate units. Bands observed at lower wavenumbers (~2040–2090 $cm^{-1}$) are characteristic of Fe(II)–CN, whereas higher-frequency bands (~2100–2160 $cm^{-1}$) correspond to Fe(III)–CN stretching vibrations.[3] The simultaneous presence or broadening of these bands indicates a mixed-valence $Fe^{2+}/Fe^{3+}$ cyanometal framework.[4] The emergence of a very broad Raman 1000–1700 $cm^{-1}$ with two intense sub-bands after the formation of Cu–aspartate–hexacyanoferrate indicates the development of a structurally disordered and heterogeneous phase, arising from, CN–Cu–Fe network formation, and mixed-valence interactions characteristic of Prussian Blue analogue systems. Simultaneously, new broad Raman features with shoulder-like profiles appear at approximately 1500 and 2300 $cm^{-1}$. The band around 1500 $cm^{-1}$ is attributed to disorder carbonaceous or nitrogen-containing species formed during electrochemical restructuring, while the feature near 2300 $cm^{-1}$ is assigned to C≡N stretching vibrations of hexacyanoferrate units interacting with copper ions.[5] The pronounced broadening and shoulder character of these bands indicate multiple coordination environments and the formation of a structurally heterogeneous copper–hexacyanoferrate phase, consistent with reports on Prussian Blue analogues and electrochemically synthesized metal hexacyanoferrates

**S6. Stability of modified nanocomposite electrode in KCl**

For investigation the stability and mas transfer, the modified electrod after 12 seccesive CV in KCl and $K_3Fe(CN)_6$ was drawn out and washed with water then placed in KCl solution. The result demonstrated the fabricated nanofiber composite of CuHCF exhibited excellent structural stability in KCl electrolyte. Not only CuHCF after washing are stable, Notably, the anodic and cathodic currents recorded in KCl after electrodeposition and subsequent washing were higher than those obtained in the solution containing $K_3Fe(CN)_6$ and KCl during the formation of the characteristic copper hexacyanoferrate redox peaks can be attributed to increase in mass transport. The corresponding data are presented in Figure S10.

**S7. Effect of KCl concentration**

The concentration of the supporting electrolyte (KCl) and the solution pH play a significant role in the electrochemical response by influencing ionic conductivity, charge compensation, and the stability of the CuHCF framework. In this work, these parameters were optimized to ensure stable and reproducible redox behavior of the CuHCF probe. Variations in KCl concentration and pH primarily affect peak currents and peak-to-peak separation, consistent

with previously reported behavior of CuHCF-based systems. The data for investigation of different concentration of KCl was exhibited in the following in Figures S11.

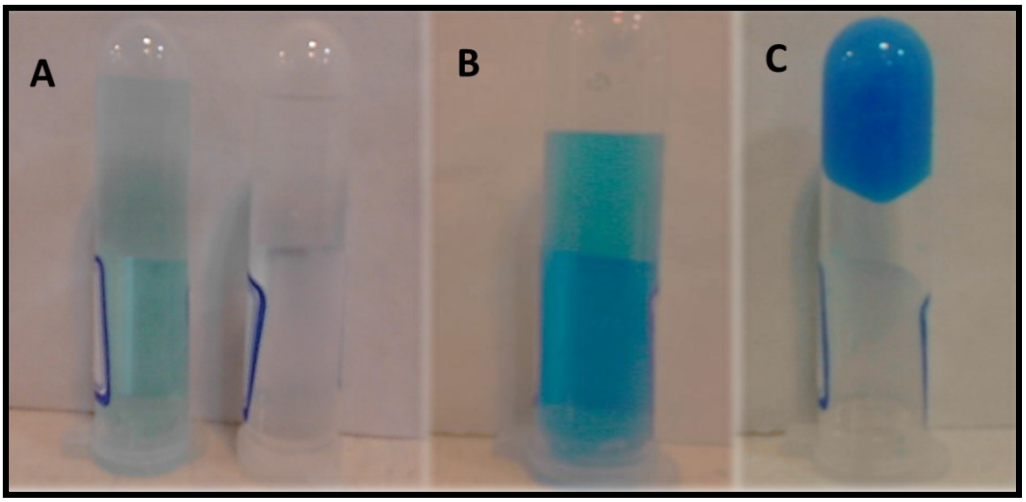


**Figure S1**. Photograph of copper and aspartic acid solution before mixing (A); 5 min after mixing (B); Gel formation after finishing the reaction(C).

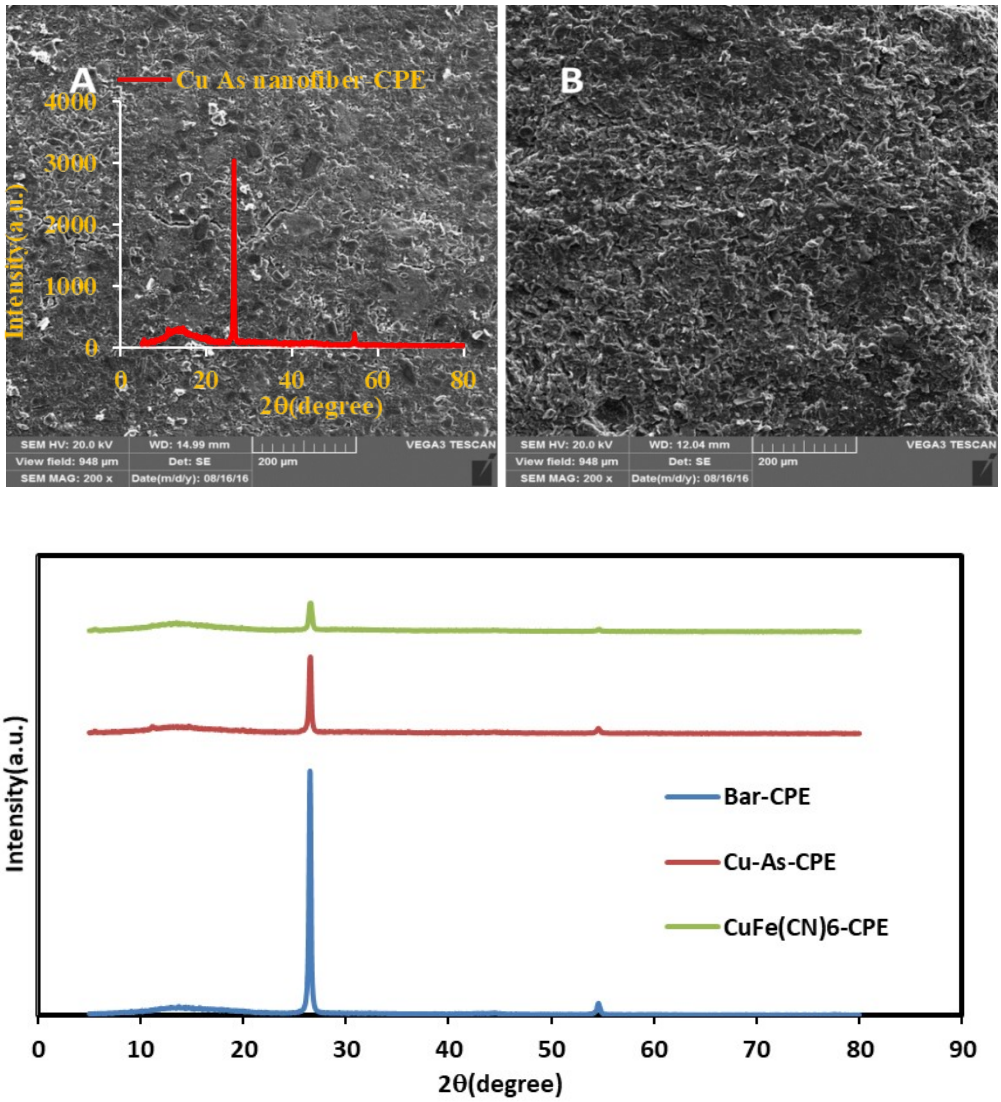


**Figure S2.** SEM image of the surface of bare-CPE with the overlay of its XRD (A), SEM image of the surface of modified Cu-L-Aspartic acid-CPE after electrodeposition of hexacyanoferrate with the overlay of its XRD(B); the XRD patterns of CPE, Cu-As-CPE and $CuFe(CN)_6$-CPE.

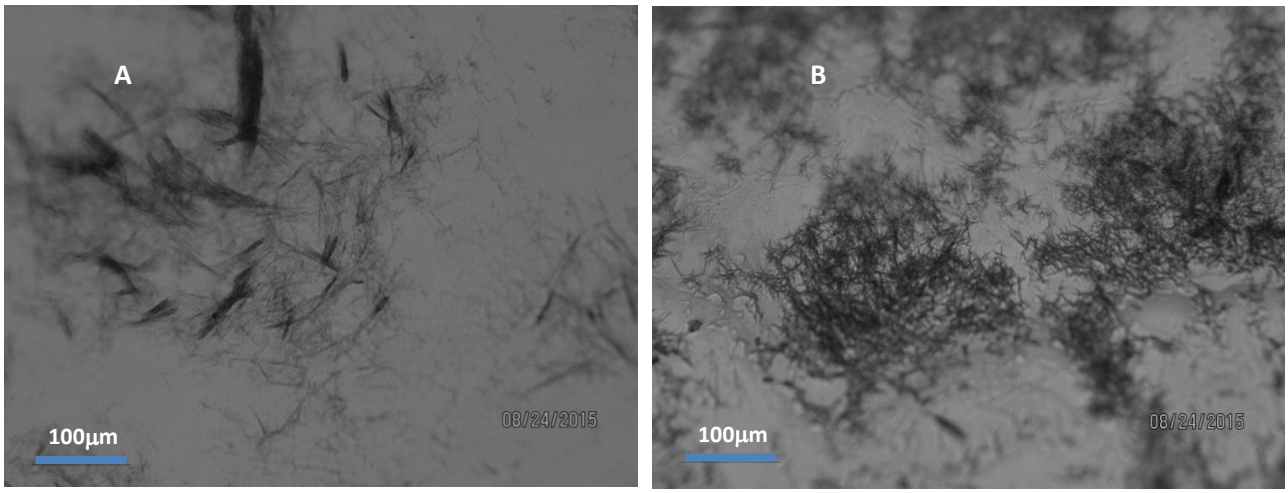


**Figure S3.** Optical photograph of Cu(II)-As nanofiber before(A) and after(B) electrodeposion of $[Fe(CN)_6]^{3-}$.

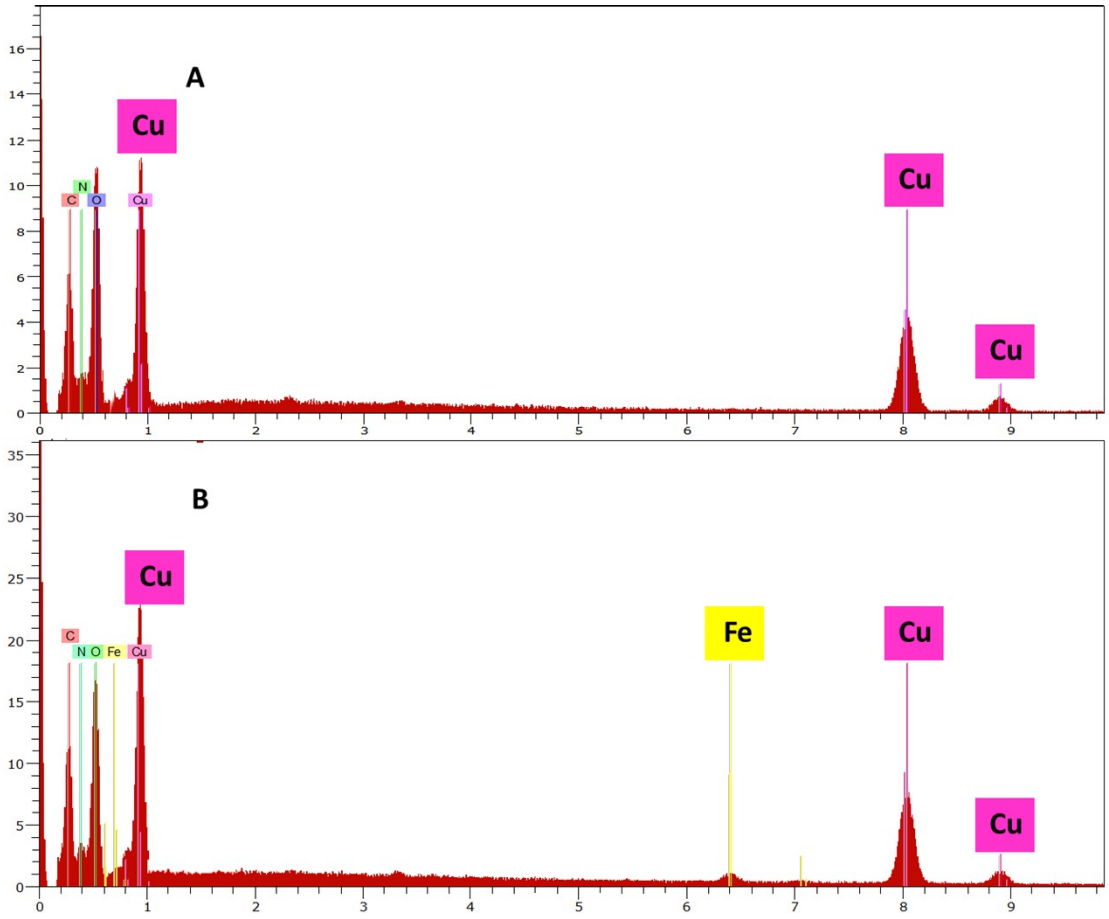


**A1**

| El | AN | Series | unn. C [wt.%] | norm. C [wt.%] | Atom. C [at.%] | Error [wt.%] |
|---|---|---|---|---|---|---|
| C | 6 | K-series | 35.93 | 28.96 | 40.58 | 4.5 |
| N | 7 | K-series | 17.12 | 13.80 | 16.58 | 2.5 |
| O | 8 | K-series | 43.63 | 35.16 | 36.99 | 5.2 |
| Cu | 29 | K-series | 27.40 | 22.09 | 5.85 | 0.8 |
| Total: | | | 124.08 | 100.00 | 100.00 | |

**B1**

| El | AN | Series | unn. C [wt.%] | norm. C [wt.%] | Atom. C [at.%] | Error [wt.%] |
|---|---|---|---|---|---|---|
| C | 6 | K-series | 25.18 | 29.61 | 41.38 | 3.0 |
| N | 7 | K-series | 13.38 | 15.74 | 18.85 | 1.8 |
| O | 8 | K-series | 27.41 | 32.23 | 33.81 | 3.2 |
| Fe | 26 | K-series | 0.90 | 1.06 | 0.32 | 0.1 |
| Cu | 29 | K-series | 18.16 | 21.36 | 5.64 | 0.5 |
| Total: | | | 85.03 | 100.00 | 100.00 | |

**Fig. S4,** EDX analysis and the corresponding data of Cu(II)-Asp nanofibers; A) and A1) before electrodeposition; B) and B1) after electrodeposition.

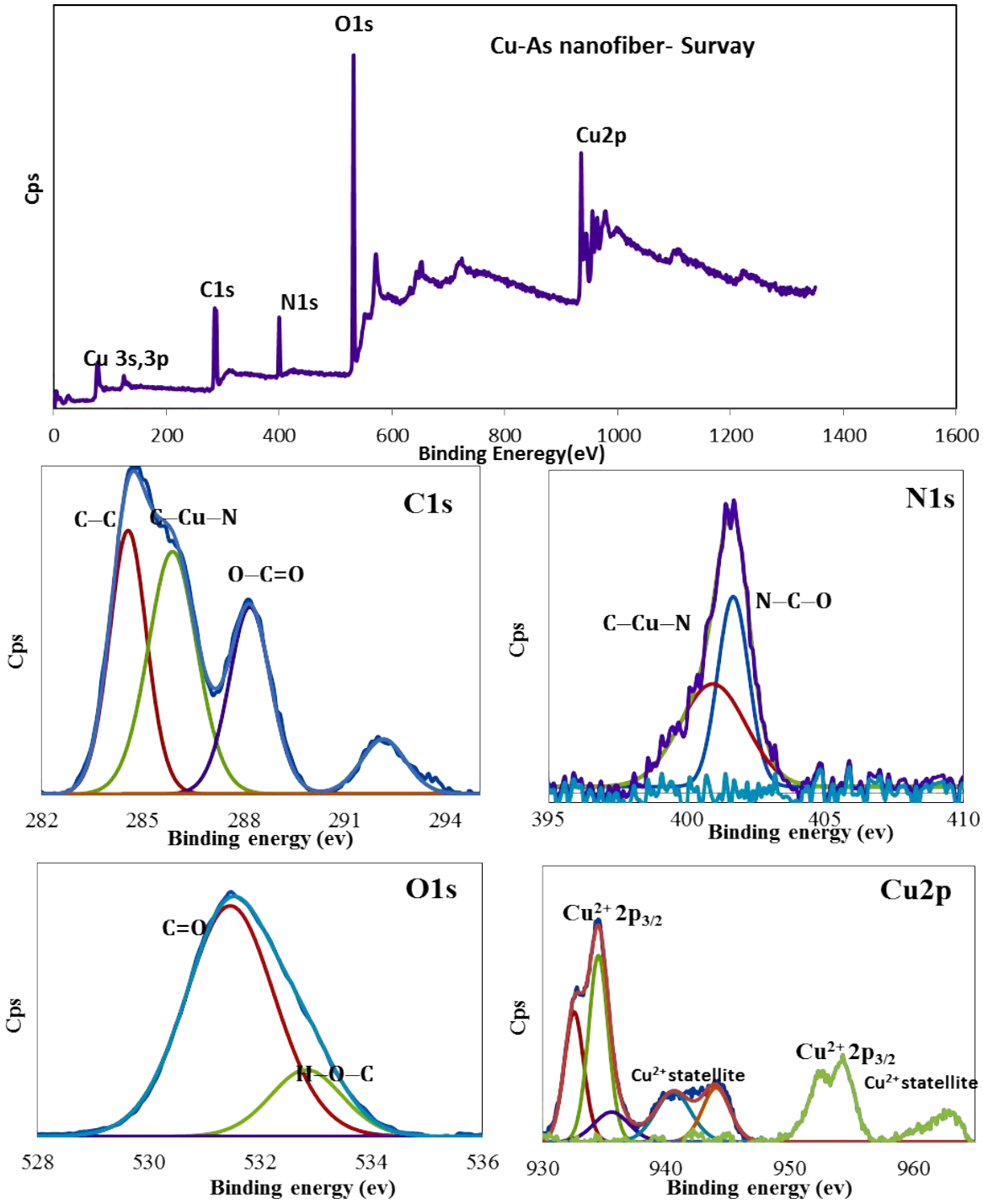


**Figure S5**. Survey XPS spectras of the Cu(II)–As nanofibers before electrodeposition of $K_3Fe(CN)_6$; high-resolution deconvoluted spectra of C1s, N1s, O1s, and Cu2p.

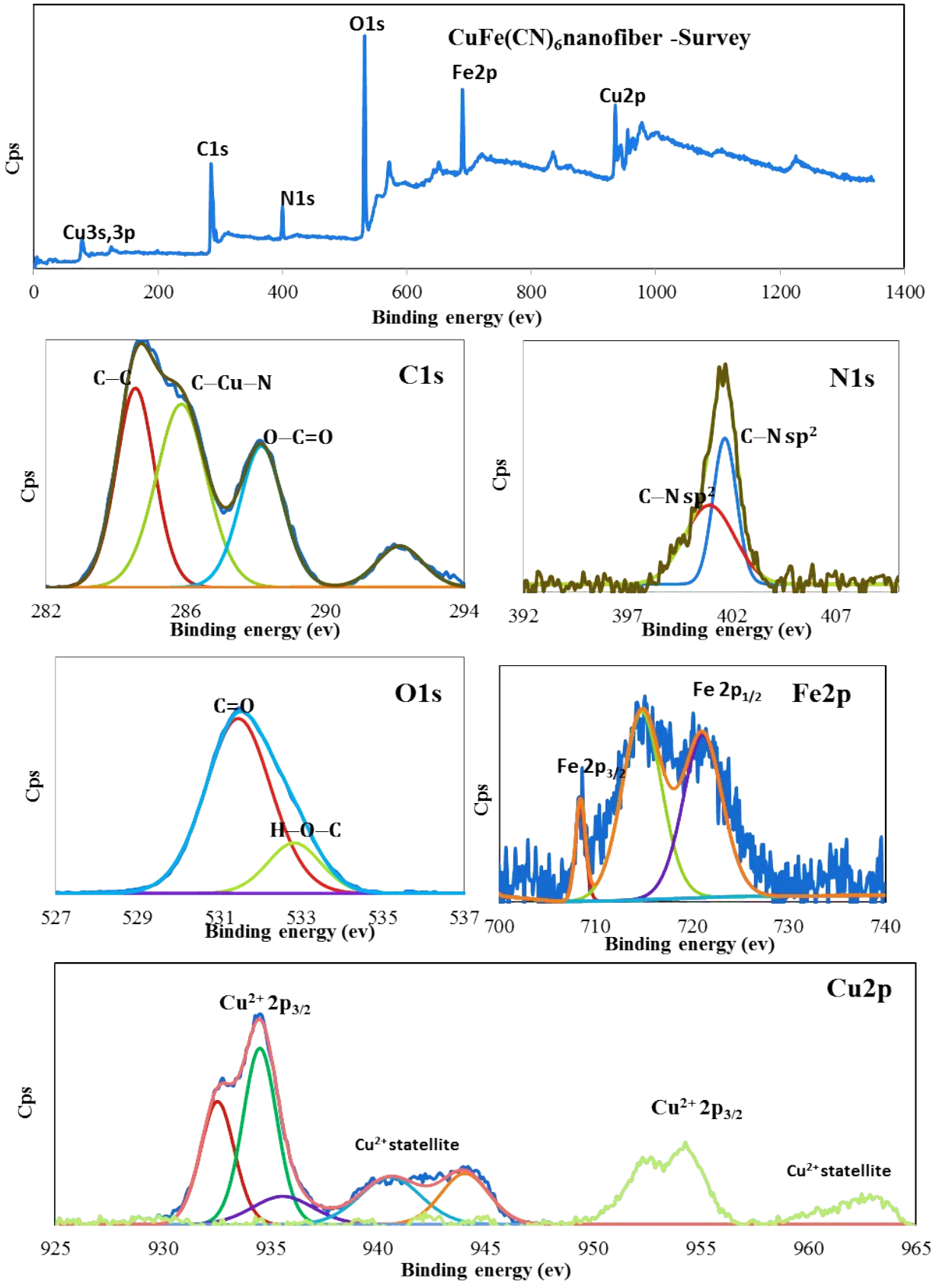


**Figure S6**. Survey XPS spectras of the Cu-As nanofibers after electrodeposition; high-resolution deconvoluted spectra of C1s, N1s, O1s, Cu2p; and Fe2p

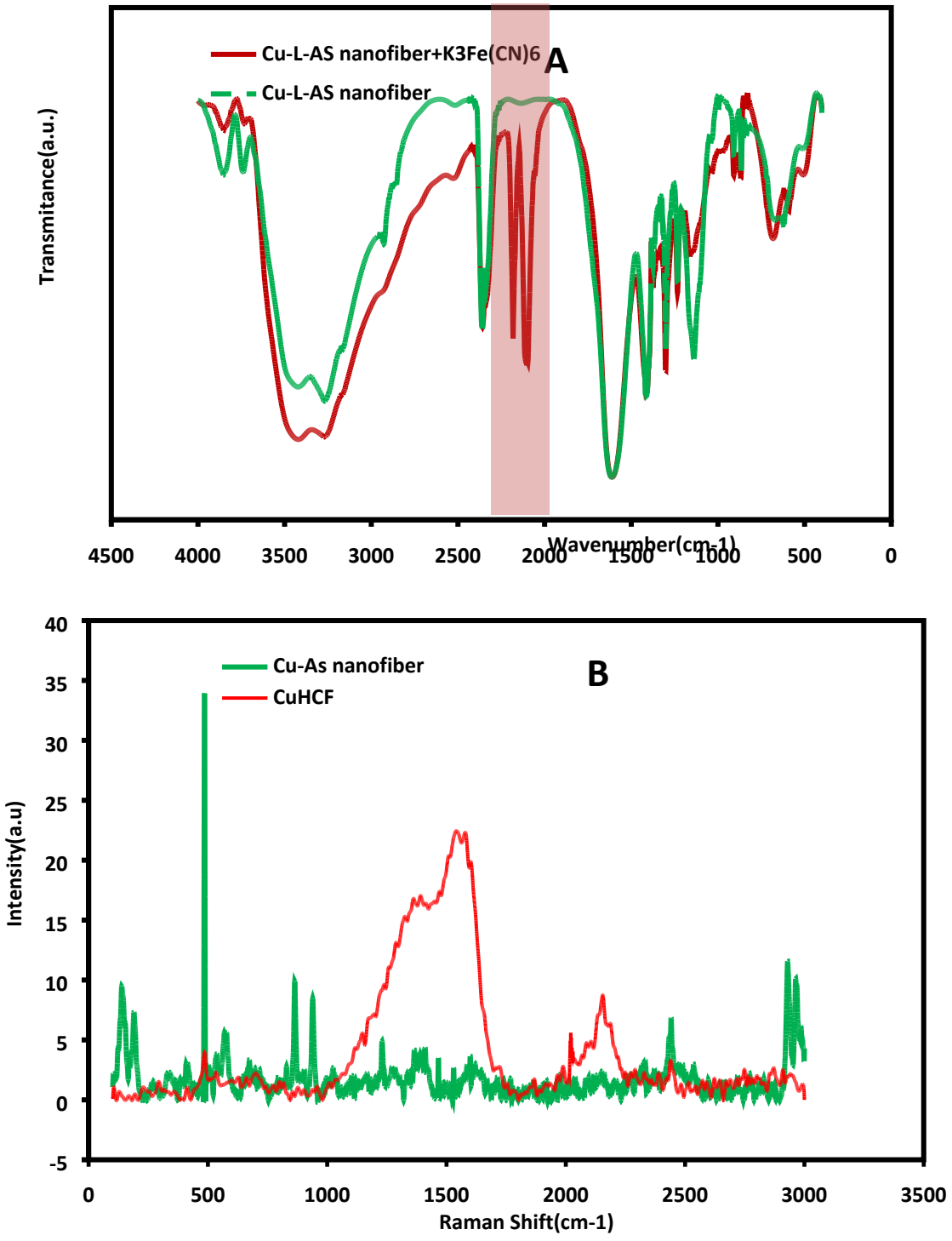


**Figure S7.** FTIR spectra of Cu(II)–L– As nanofiber before and after electrodeposition(Cu(II)–L– As nanofiber-$Fe(CN)_6$)(A); the raman spectra of Cu-L-Aspartic acid nanofiber (green line), and Cu-L-Aspartic acid nanofiber after electrodeposition of $K_3Fe(CN)_6$(RED line)(B).

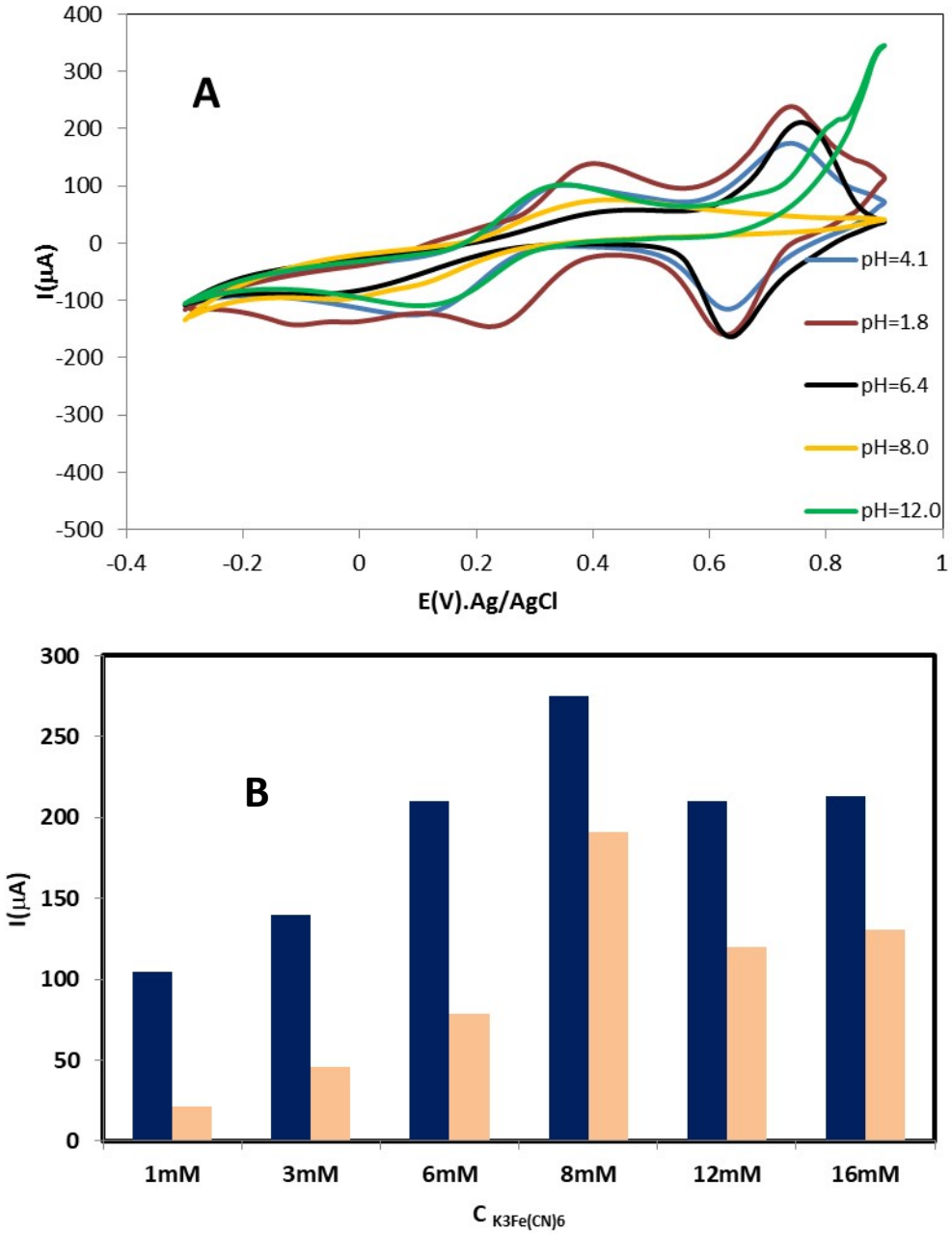


**Figure S8.** Cyclic voltammograms of the modified electrode in different pH (A); the oxidation peak currents and background currents in different concentration(B) of $K_3Fe(CN)_6$ solution containing 0.1 M KCl; scan rate 50 mV/s.

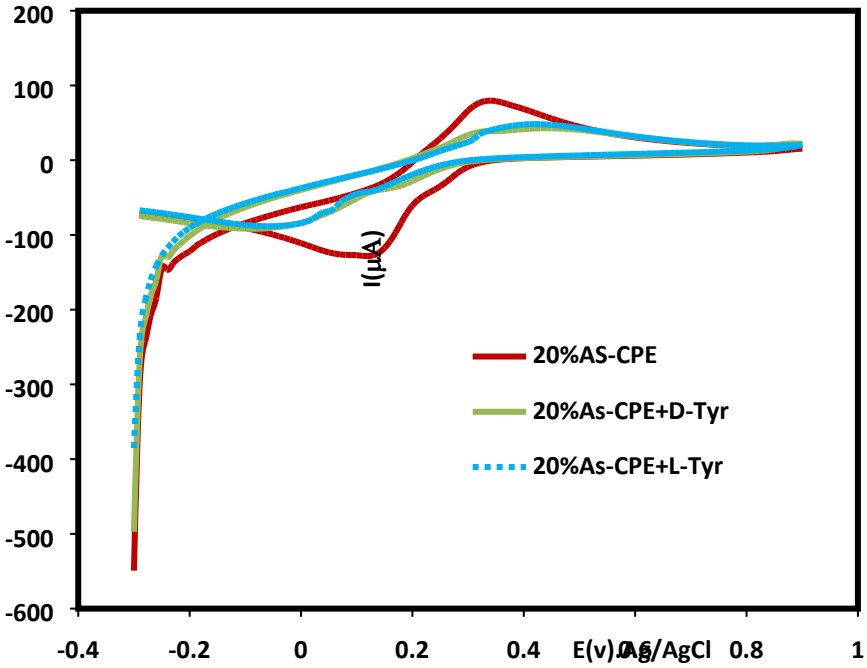


**Figure S9.** Cyclic voltammogram of Aspartic acid-modified CPE(red solid line), incubation in D-Tyr(green solid line) and incubation in (blue dotted line) in $K_3Fe(CN)_6$ solution. 5mM and 100mM of KCl after 15cycles.

**Table S1.** Comparative Table of Electrochemical Sensors for L- and D Tyrosine Determination.

| **Electrode Modifier** | **Method** | **Limit of Detection (LOD)** | **Electroanalytical Parameters** | **Reference** |
|---|---|---|---|---|
| SSSS-TCA-MWCNTs-CPE | DPV | 2.1–140 μM | 0.51 μM (L-TYR), 0.264 μM (D-TYR) | [6] |
| β-Cyclodextrin / Graphene Quantum Dots modified electrode | ECL | - | $6.07 \times 10^{-9}$ M(L-TYR); $1.03 \times 10^{-7}$ M D-TYR) | [7] |
| CyA/GCE Cysteic acid | DPV | - | - | [8] |
| Bis-aminosaccharides composite (CS-GalN) / GCE | SWV | 0.01–1.00 mM | 0.65 μM (L-TYR); 0.86 μM (D-TYR)) | [9] |
| $Cu_2$-α-CD-CS/GCE | DPV | - | - | [10] |
| L-Cys-Au-$Fe_3O_4$/MGCE | SWV | 1–125 μM | 0.021 μM (L-TYR), 0.084 μM (D-TYR) | [11] |
| SS-CS/GCE | SWV | 10–100 μM | 0.35 μM (L-TYR), 0.42 μM (D-TYR) | [12] |
| Cu-As-nanofiber/hexacyanoferrate | CV-indirect | 2.5-300 μM | $1.72 \times 10^{-6}$ (L-TYR), $8.48 \times 10^{-7}$(D-TYR) | This Work |

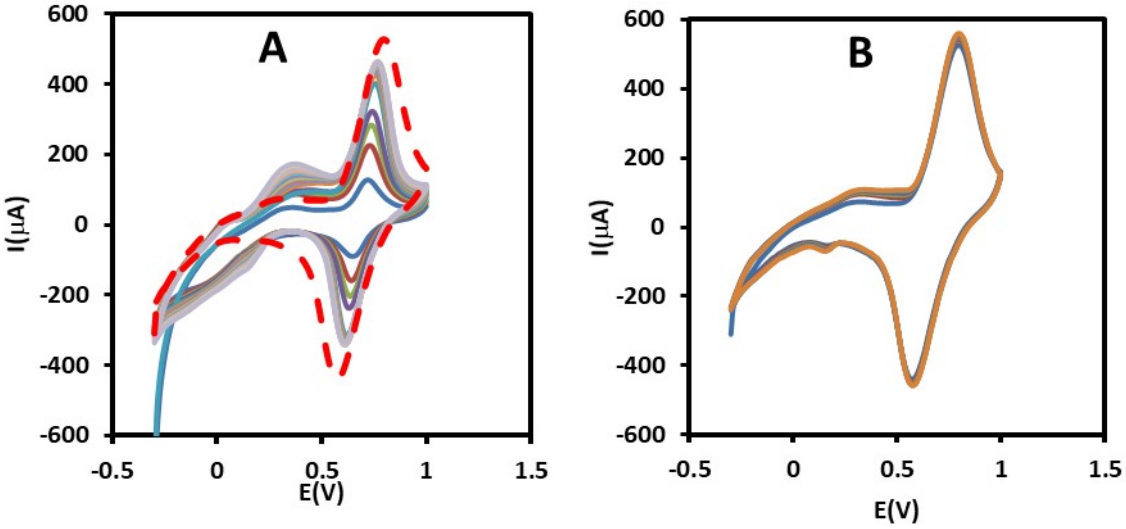
A
B
600
400
200
0
-200
-400
-600
I(μA)
-0.5
0
0.5
1
1.5
E(V)

**Figure S10**. A. Cyclic voltammograms of Cu-As-modified CPE in 8mM $K_3Fe(CN)_6$ , 12 cycle(solid line) and the dashed line in 0.1M KCl after washing of the electrodeposited CuHCF. B.CuHCF modified electrode after washing in 0.1 M KCl 6cycles

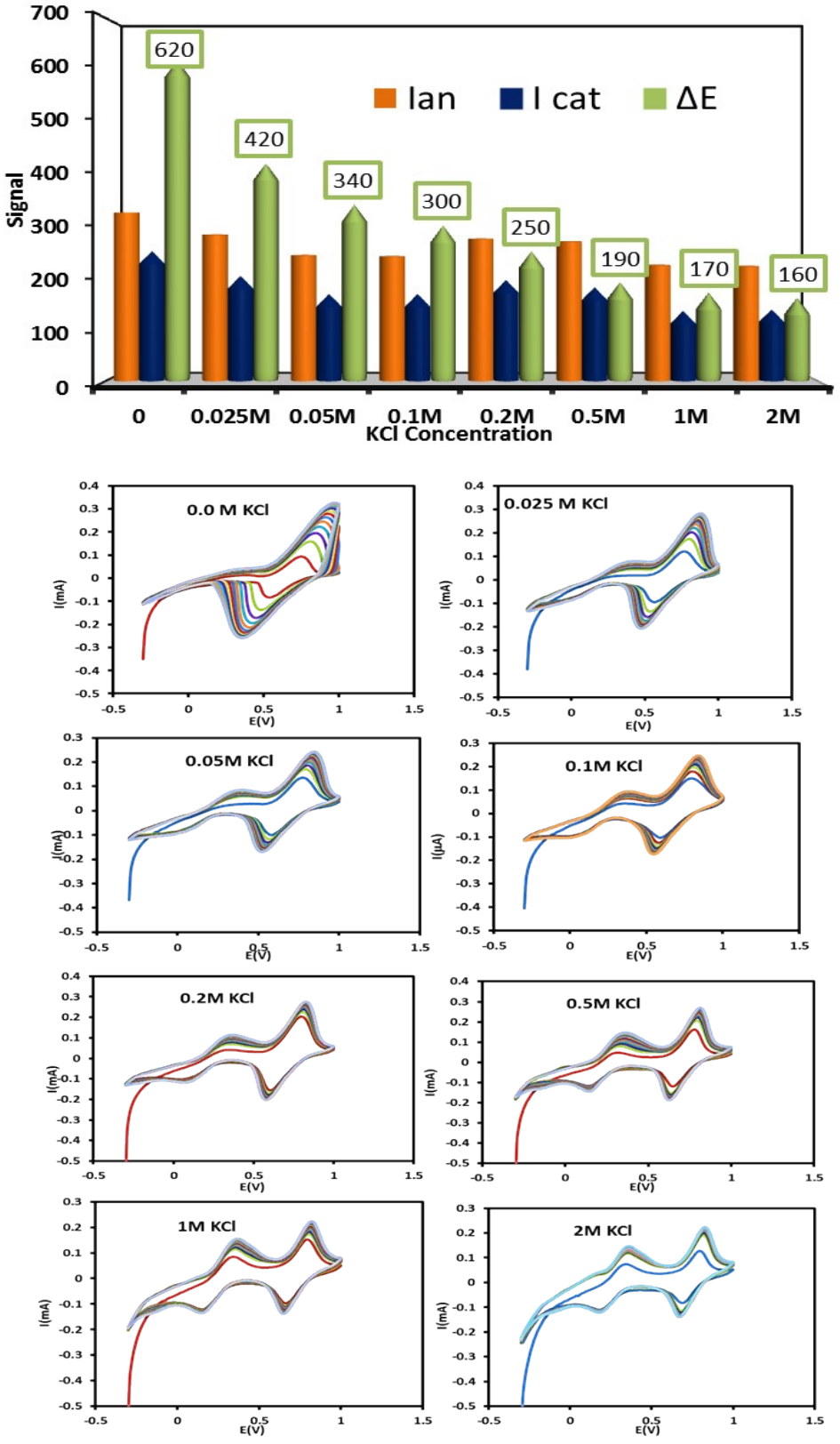


**Figure S11.** Effect of different concentrations of KCl on redox peak of CuHC, Cyclic voltammogram of CuHCF formation by 12 CV Cycles in various concentration of KCl**.**

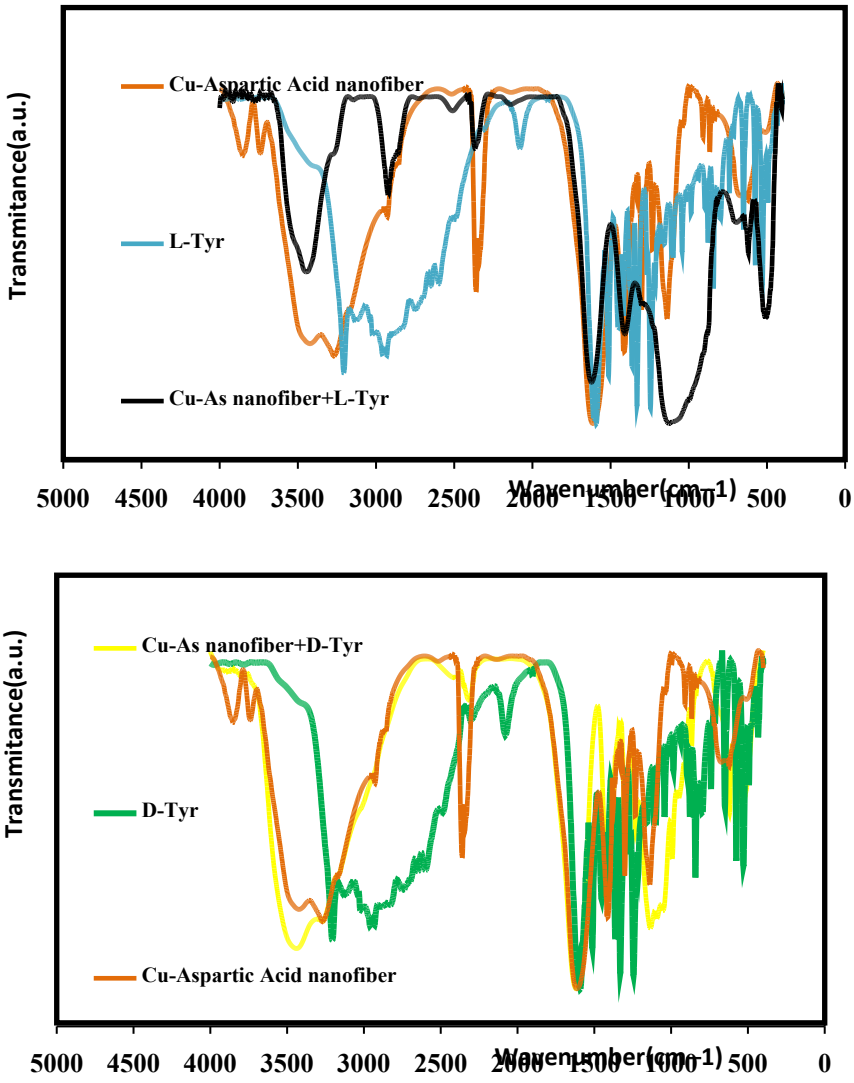


**Figure S12.** FTIR spectra of Cu(II)–L– As nanofiber before and after interaction with L and D- Tyr and pure Tyr.

**References:**

[[1] X. Gao, Y. Lu, M. Liu, S. He, W. Chen, *J. Mater. Chem. C* **2015**, 3, 4050.

[2] A. Gopalakrishnan, N. Vishnu, S. Badhulika, *J. Electroanal. Chem.* **2019**, 834, 187.

[3] D. O. Ojwang, J. Grins, D. Wardecki, M. Valvo, V. Renman, L. Häggström, T. Ericsson, T. r. Gustafsson, A. Mahmoud, R. P. Hermann, *Inorg. chem.* **2016**, 55, 5924.

[4] K. Nakamoto, *Infrared and Raman spectra of inorganic and coordination compounds, part B: applications in coordination, organometallic, and bioinorganic chemistry*, John Wiley & Sons, **2009**.

[5] K. R. Dunbar, R. A. Heintz, *Prog. inorg. chem.***1997**, 45, 283.

[6] S. S. Upadhyay, M. Dar, N. S. Gadhari, J. V. Gholave, K. S. Bhole, D. Manoj, P. K. Kalambate, *J. Electrochem. Soc.* **2025**.

[7] S. Dong, Q. Bi, C. Qiao, Y. Sun, X. Zhang, X. Lu, L. Zhao, *Talanta* **2017**, 173, 94.

[8] R. Nie, X. Bo, H. Wang, L. Zeng, L. Guo, *Electrochem. commun.* **2013**, 27, 112.

[9] J. Zou, J.-G. Yu, *Anal. Chim. Acta* **2019**, 1088, 35.

[10] Y. Tao, F. Chu, X. Gu, Y. Kong, Y. Lv, L. Deng, *Sensors &Actuators B: Chemical* **2018**, 255, 255.

[11] X. Shi, Y. Wang, C. Peng, Z. Zhang, J. Chen, X. Zhou, H. Jiang, *Electroch. Acta* **2017**, 241, 386.

[12] J. Zou, X.-Q. Chen, G.-Q. Zhao, X.-Y. Jiang, F.-P. Jiao, J.-G. Yu, *Talanta* **2019**, 195, 628.

ss